Implementation of Nonquasi-Static Effects in Compact Bipolar Transistor Models

Sergey V. Cherepko, *Student Member, IEEE,* and James C. M. Hwang, *Fellow, IEEE*

***Abstract*—Large-signal implementation of nonquasi-static (NQS) effects in bipolar transistors is reviewed. An approach is proposed to introduce first-order NQS correction to typical quasi-static phenomenological models. Both charge- and non-charge-conserving implementations are considered. The resulted large-signal equivalent-circuit model compares well with the two-dimensional physical model in simulating HBT transient response under high-current operations. The present approach advances the state-of-the-art by allowing arbitrary bias dependence of transit times in large-signal NQS models.**

***Index Terms*—Bipolar transistors, charge carrier processes, HBTs, nonlinear circuits, semiconductor device modeling.**

I. Introduction

COMPACT models of bipolar transistors often fail as the operating frequency approaches the cutoff frequency and the transistor can no longer follow external excitations instantaneously. This delay is usually referred to as the nonquasi-static (NQS) effect. As bipolar transistors are increasingly used at a significant fraction of the cutoff frequency, it is important to account for the NQS effect in a concise manner so that it can be readily implemented in a compact model.

The NQS effect can be accounted for by using a distributed equivalent circuit [1], [2]. However, this leads to complicated models that are difficult to extract from measured data. A practical alternative is to estimate the NQS effect analytically and to modify existing compact models to mimic the estimated behavior. For bipolar junction transistors (BJTs), analytical expressions have been derived to model carrier transport through the quasi-neutral base, emitter [3]–[7], and depleted collector [8]. Most of the analysis to date concentrates on small-signal operations. For large-signal operations, transit times and other small-signal model parameters vary with the bias, which makes large-signal equivalent-circuit implementation of the NQS effect very complicated. Implementation approaches proposed to date are either limited to bias-independent time constants [3]–[6], [9] or require access to the circuit simulator engine [10]. Reference [11] does not include circuit implementation at all.

The goal of this paper is a simple and systematic approach for implementing the NQS effect in a large-signal equivalent-circuit model that allows for arbitrary bias dependence of time constants. Section II summarizes the status of small-signal NQS modeling in BJTs and compares it with quasi-static (QS) modeling. Section III illustrates the present approach to large-signal implementation and discusses charge-conservation issues. The implementation is then used to model HBT transient response in Section IV. To validate the present approach, the modeled HBT transient response is compared with that simulated by using a two-dimensional physical device model.

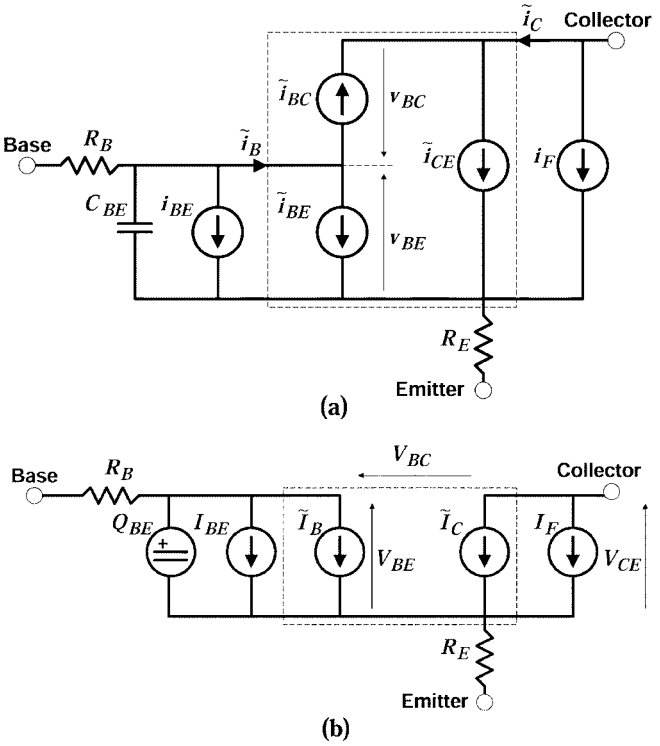

Fig. 1. (a) Small- and (b) large-signal equivalent circuits of the BJT in a forward active regime. High-frequency dispersive components are enclosed in dashed boxes.

II. Small-Signal NQS Effects

This section summarizes QS and NQS expressions for BJT small-signal base and collector currents. The BJT is assumed to operate in the forward active regime. The small-signal equivalent circuit of the intrinsic HBT is depicted in Fig. 1(a). Currents in Fig. 1 are separated into low-and high-frequency components. Low-frequency currents $i_{\rm BE}$ and i_F represent base recombination and collector transport, respectively. Both $i_{\rm BE}$ and i_F are assumed to follow the small-signal base–emitter voltage $\nu_{\rm BE}$ instantaneously. High-frequency currents $\tilde{i}_{\rm BE}$ and $\tilde{i}_{\rm CE}$ account for electron transport through the quasi-neutral base. $\tilde{i}_{\rm BE}$ and $\tilde{i}_{\rm CE}$

Manuscript received April 20, 2003. This work was supported in part by the Center for Optical Technologies, Lehigh University.

The authors are with the Department of Electrical Engineering, Lehigh University, Bethlehem, PA 18015 USA (e-mail: svcher@lehigh.edu).

Digital Object Identifier 10.1109/TMTT.2003.819780

TABLE I
APPROXIMATIONS OF $\tilde{i}_{\rm BE}$ AND $\tilde{i}_{\rm CC}$

Model	$\tilde{i}_{BE}$	$\tilde{i}_{CC}$
SGP [12] VBIC [9]	$i_F \cdot \tau_F s$	$i_F \cdot \exp(-\tau_\varphi s)$
MEXTRAM [10]	$i_F \cdot \tau_F s$	$i_F \cdot (1-\tau_\varphi s)$
HICUM [11]	$i_F \cdot \tau_F s \exp(-\tau_D s)$	$i_F \cdot \exp(-\tau_\varphi s)$
[3], [5]	$\frac{i_F \cdot \tau_F s}{1+\tau_D s}$	$\frac{i_F \cdot \exp(-\tau_\varphi s)}{1+\tau_D s}$
[6], [7]	$\frac{i_F \cdot \tau_F s}{1+\tau_D s}$	$\frac{i_F}{1+\tau_D s}$

can have strong frequency dependence, as will be discussed in Section II-A. These dispersive quantities are denoted by tildes throughout this paper. The combined current

$$\tilde{i}_{\rm CC} = i_F + \tilde{i}_{\rm CE} \tag{1}$$

represents the current of the electrons leaving the base and entering the collector. $\tilde{i}_{\rm BC}$ arises from the electron transport through the base–collector depletion region and will be dealt with in Section II-B. Finally, dispersive terminal currents $\tilde{i}_B$ and $\tilde{i}_C$, of which large-signal implementation is the main focus of this paper, will be derived in Section II-C. Notice that

$$\tilde{i}_B = \tilde{i}_{\rm BE} + \tilde{i}_{\rm BC}. \tag{2}$$

$$\tilde{i}_C = \tilde{i}_{\rm CE} - \tilde{i}_{\rm BC}. \tag{3}$$

The displacement current through the base–emitter depletion capacitance $C_{\rm BE}$, although having well-defined frequency dependence, is not included in $\tilde{i}_B$. This is because $C_{\rm BE}$ depends only on the base–emitter voltage and can be readily incorporated in a large-signal equivalent circuit as a conventional charge source.

A. Base Transport

Small-signal base and collector currents due to transport through the quasi-neutral base are subjects of numerous publications. Closed-form expressions are available for the simple case of low injection, uniform base doping, and constant built-in electric field [3]–[5]. In other cases, the solution can be derived as an infinite series of multiple integrals [6], [7]. These exact small-signal solutions are too complicated to be implemented in compact models. Table I summarizes the approximations used in popular compact models, as well as proposed in the literature.

In Table I, s is the complex frequency $j\omega$. τ_F, τ_φ, and τ_D are small-signal time constants. τ_F is the forward transit time without contribution from the collector transit time. τ_φ accounts for excess phase delay and magnitude degradation of $\tilde{i}_{\rm CC}$ in the four popular models. τ_φ originates from partitioning the base charge between the emitter and collector [13], which is not considered as an NQS effect in this study. Since the partitioning of the base charge has no effect on $\tilde{i}_{\rm BE}$, no additional correction to $\tilde{i}_{\rm BE}$ is implemented in the popular models, except HICUM [11]. This is in contrast with the more accurate approximations of [3], [5]–[7], where τ_D is used to account for NQS effects on both $\tilde{i}_{\rm BE}$ and $\tilde{i}_{\rm CC}$.

The QS and NQS expressions in Table I can be further simplified by expanding the exponentials and dropping higher order terms of s as follows:

$$\tilde{i}_{\rm BE}^{\rm QS} = i_F \cdot \tau_F s \tag{4}$$

$$\tilde{i}_{\rm CE}^{\rm QS} = \tilde{i}_{\rm CC} - i_F = -i_F \cdot \tau_\varphi s \tag{5}$$

$$\tilde{i}_{\rm BE}^{\rm NQS} = \frac{i_F \cdot \tau_F s}{1+\tau_D s} \tag{6}$$

$$\tilde{i}_{\rm CE}^{\rm NQS} = \tilde{i}_{\rm CC} - i_F = -\frac{i_F \cdot \tau_D s}{1+\tau_D s}. \tag{7}$$

Note that $\tilde{i}_{\rm CE}^{\rm NQS}$ follows the simpler form of [6] and [7] instead of the exponential form of [3] and [5]; the latter may only give marginal improvement in accuracy [14], [15].

B. Collector Transport

After leaving the quasi-neutral base, electrons travel in the collector depletion region before reaching the collector electrode. Depending on the collector design and operating condition, the collector transit time may exceed the base transit time. Therefore, the NQS effect on collector transport may be present at lower frequencies than that of base transport. Assuming that electrons travel through the collector with saturated velocity, the small-signal base current generated by the collector transport can be expressed as [8]

$$\tilde{i}_{\rm BC} = \tilde{i}_{\rm CC}\left(1 - \frac{1-\exp(-2\tau_C s)}{2\tau_C s}\right) \tag{8}$$

where $2\tau_C$ is the time it takes an electron to drift through the collector depletion region. The QS approximation of (8) is simply its first-order expansion with respect to s, while the NQS approximation can be derived in a rational form as follows:

$$\tilde{i}_{\rm BC}^{\rm QS} = \tilde{i}_{\rm CC} \cdot \tau_C s \tag{9}$$

$$\tilde{i}_{\rm BC}^{\rm NQS} = \frac{\tilde{i}_{\rm CC} \cdot \tau_C s}{1+\dfrac{2\tau_C s}{3}}. \tag{10}$$

Under high currents, the BJT may suffer from the Kirk (base push-out) effect. In this case, the collector transit time also accounts for electron diffusion in the pushed-out base region.

C. Combined Small-Signal Model

The formulas in Sections II-A and B can be combined to obtain terminal dispersive currents $\tilde{i}_B$ and $\tilde{i}_C$, with the added effect of the base–collector depletion capacitance $C_{\rm BC}$. The small-signal current through $C_{\rm BC}$ is simply $\nu_{\rm BC}C_{\rm BC}$; $\nu_{\rm BC}$ being the small-signal base collector voltage. Under large signal, $C_{\rm BC}$ depends not only on the base–collector voltage, but also the collector current [16]. Therefore, the large-signal implementation of $C_{\rm BC}$ is not trivial.

From (1), (2), (4), (5), and (9), and after dropping the $(\tau s)^2$ term

$$\tilde{i}_B^{\rm QS} = i_F \cdot (\tau_F + \tau_C)s + v_{\rm BC} \cdot C_{\rm BC} s. \tag{11}$$

From (1), (3), (5), and (9)

$$\tilde{i}_C^{\rm QS} = -i_F \cdot (\tau_\varphi + \tau_C)s - v_{\rm BC} \cdot C_{\rm BC} s. \tag{12}$$

From (1), (2), (6), (7), and (10)

$$\tilde{i}_B^{\rm NQS} = \frac{i_F \cdot (\tau_F + \tau_C)s}{1 + \left(\tau_D + \frac{2\tau_C}{3}\right)s} + v_{\rm BC} \cdot C_{\rm BC} s. \qquad (13)$$

From (1), (3), (7), and (10)

$$\tilde{i}_C^{\rm NQS} = \frac{i_F \cdot (\tau_F + \tau_C)s}{1 + \left(\tau_D + \frac{2\tau_C}{3}\right)s} - v_{\rm BC} \cdot C_{\rm BC} s. \qquad (14)$$

III. Large-Signal Implementation

The large-signal equivalent circuit of the BJT is shown in Fig. 1(b). Low-frequency currents $I_{\rm BE}$ and I_F are conventional nonlinear voltage-controlled current sources, which are related to the small-signal currents of Section II in the conventional manner

$$i_{\rm BE} = v_{\rm BE} \cdot \frac{dI_{\rm BE}}{dV_{\rm BE}} = v_{\rm BE} \cdot g_{\rm BE} \qquad (15)$$

$$i_F = v_{\rm BE} \cdot \frac{dI_F}{dV_{\rm BE}} = v_{\rm BE} \cdot g_m. \qquad (16)$$

Notice that large- and small-signal parameters are distinguished by upper and lower cases throughout this paper. The charge source that models the base–emitter depletion capacitance is defined as in the following:

$$Q_{\rm BE} = \int C_{\rm BE} dV_{\rm BE}. \qquad (17)$$

Since $Q_{\rm BE}$, $I_{\rm BE}$, and I_F can be readily implemented, this section concentrates on implementation of dispersive currents $\tilde{I}_B$ and $\tilde{I}_C$. QS and NQS approximations are discussed in Sections III-A and B, respectively.

A. QS Approximation

From (11) and (12), both the small-signal base and collector currents have the same general form

$$\tilde{\tilde{i}} = i_F \cdot \tau s + v_{\rm BC} \cdot C_{\rm BC} s \qquad (18)$$

where $\tilde{\tilde{i}}$ represents either the base or collector dispersive current and τ is the corresponding small-signal time constant. Equation (18) can be converted into the time domain by applying the inverse Laplace transformation

$$\tilde{I} = \tau \cdot \frac{dI_F}{dt} + C_{\rm BC} \cdot \frac{dV_{\rm BC}}{dt}. \qquad (19)$$

The transformation from (18) to (19) is valid only if (18) is linear with constant τ and $C_{\rm BC}$. However, (19) can be transformed into (18) even if τ and $C_{\rm BC}$ are bias dependent. This can be verified by expanding (19) under a small-signal excitation

$$\begin{aligned}\delta\tilde{I} &= (\tau + \delta\tau)\frac{d(I_F + \delta I_F)}{dt} \\ &\quad + (C_{\rm BC} + \delta C_{\rm BC})\frac{d(V_{\rm BC} + \delta V_{\rm BC})}{d} \\ &\approx \tau \frac{d\delta I_F}{dt} + C_{\rm BC}\frac{d\delta V_{\rm BC}}{dt} \end{aligned} \qquad (20)$$

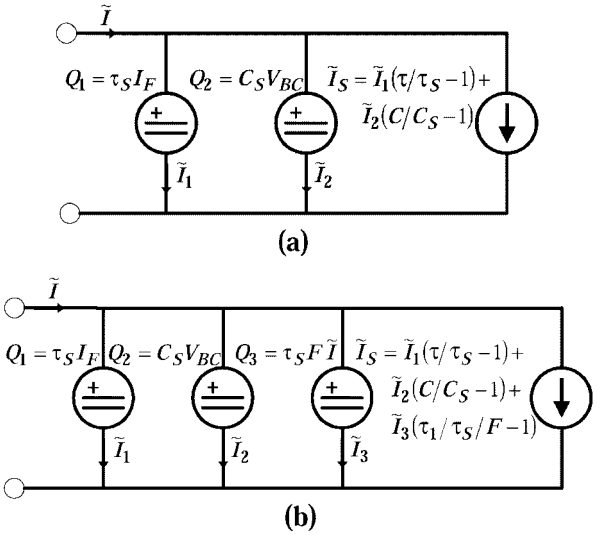

Fig. 2. (a) QS and (b) NQS large-signal implementation of base or collector dispersive current with τ_S and C_S as normalization factors. Function F is defined in (27).

where δ indicates small-signal variation and the approximation is arrived at by dropping δ^2 terms. The Laplace transform of (20) is exactly (19).

Compact models normally treat $\tilde{I}$ as current through a charge source $Q(I_F, V_{\rm BC})$, thus ensuring charge conservation for the corresponding terminal

$$\tilde{I} = \frac{dQ}{dt} = \frac{\partial Q}{\partial I_F} \cdot \frac{dI_F}{dt} + \frac{\partial Q}{\partial V_{\rm BC}} \cdot \frac{dV_{\rm BC}}{dt}. \qquad (21)$$

$Q(I_F, V_{\rm BC})$ can be obtained by comparing (19) and (21) and solving for Q

$$\frac{\partial Q}{\partial I_F} = \tau \quad \frac{\partial Q}{\partial V_{\rm BC}} = C_{\rm BC}. \qquad (22)$$

Equation (22) can be solved only if

$$\frac{\partial \tau}{\partial V_{\rm BC}} = \frac{\partial C_{\rm BC}}{\partial I_F}. \qquad (23)$$

Equation (23) may not hold given arbitrary $\tau(I_F, V_{\rm BC})$ and $C_{\rm BC}(I_F, V_{\rm BC})$. In case (23) does not hold, one may still attempt to derive $Q(I_F, V_{\rm BC})$ so that it matches (22) as closely as possible. Such a charge–source implementation may be desirable when device physics dictates charge conservation, e.g., for the BJT base terminal or the FET gate terminal. However, since (22) may not be exact, the resulted large-signal model may not reproduce the bias dependence of small-signal characteristics.

When charge conservation is not assured, such as in the case of a BJT collector terminal or FET drain terminal [17], an alternative approach is to model (19) directly with parallel charge and current sources. The charge sources Q_1 and Q_2 in Fig. 2(a) are used to obtain the corresponding derivatives in (19) and the current source $\tilde{I}_S$ scales the derivatives to arrive at $\tilde{I}$. This nonlinear capacitance approach has an advantage over the charge–source approach in that it explicitly tracks the bias dependence of τ and $C_{\rm BC}$, thus ensuring bilateral correlation between small- and large-signal models. The obvious disadvantage is that it may not conserve charge.

B. NQS Approximation

Similarly to (18), the dispersive components of the small-signal base and collector currents (13) and (14) can be generalized as

$$\tilde{i} = \frac{i_F \cdot \tau s}{1+\tau_1 s} + v_{\rm BC} \cdot C_{\rm BC} s \tag{24}$$

where τ_1 is the new bias-dependent small-signal parameter in addition to those present in (18). This type of small-signal response represents a first-order NQS correction to the BJT model [6], [7] or the FET model [18]. Equation (24) can be readily transformed into a large-signal model in the case of bias-independent τ, τ_1, and $C_{\rm BC}$, as shown in [3]–[6] and [9]. Bias-dependent small-signal parameters of an FET were treated in [11] and [19], but no circuit representation was proposed.

Equation (24) can be made linear with respect to s by multiplying both sides with $1+\tau_1 s$ while dropping s^2 terms

$$\tilde{i} + \tilde{i} \cdot \tau_1 s = i_F \cdot \tau s + v_{\rm BC} \cdot C_{\rm BC} s. \tag{25}$$

Based on the same arguments as in Section III-A, (25) can be converted into the time domain as follows:

$$\tilde{I}(t) + \tau_1 \frac{d\tilde{I}(t)}{dt} = \tau \frac{dI_F(t)}{dt} + C_{\rm BC} \frac{dV_{\rm BC}(t)}{dt}. \tag{26}$$

The right-hand side of (26) is the same as that of (19). Thus, the NQS correction is through the derivative (damping) term on the left-hand side of (26). However, this term is not uniquely defined. It can be shown that any expression of the form

$$\frac{\tau_1}{F} \frac{d(F\tilde{I})}{dt} \tag{27}$$

where F is an arbitrary function of bias, produces the desired small-signal contribution $\tilde{i} \cdot \tau_1 s$ in (25). Indeed, linear expansion of (27) under small-signal excitation yields the inverse Laplace transformation of $\tilde{i} \cdot \tau_1 s$

$$\delta\left[\frac{\tau_1}{f}\frac{d(F\tilde{I})}{dt}\right] = \left[\frac{\tau_1}{F} + \delta\left(\frac{\tau_1}{F}\right)\right]\left(\tilde{I}\frac{d\delta F}{dt} + F\frac{d\delta\tilde{I}}{dt}\right) \approx \tau_1 \frac{d\delta\tilde{I}}{dt}. \tag{28}$$

Note that, by definition, both δ^2 and the time-invariant part of $\tilde{I}$ are equal to zero.

The NQS (26) converges to the QS (19) when the change in $\tilde{I}$ becomes slow and $\tau_1(d\tilde{I}/dt) \ll \tilde{I}$. Therefore, the discussion of charge–source implementation in Section III-A is applicable here as well. The large-signal implementation of (26) depends on whether or not charge conservation is needed. If it is, then the right-hand side of (26) allows charge–source representation and the corresponding charge function $Q(I_F, V\mathrm{BC})$ can be found by solving (22). The damping term in (26) can be transformed into a full time-derivative by choosing $F = \tau_1$ in (27) so that (26) becomes

$$\tilde{I}(t) = \frac{d}{dt}\left[Q(I_F, V_{\rm BC}) - \tau_1 \tilde{I}(t)\right]. \tag{29}$$

EMITTER CONTACT			
Emitter cap	$In_{0.6}Ga_{0.4}As$	40 nm, n, $2\cdot10^{19}$	
Emitter 1	GaAs	120 nm, n, $1\cdot10^{19}$	
Emitter 2	$In_{0.48}Ga_{0.52}P$	50 nm, n, $3\cdot10^{17}$	BASE CONTACT
Base	GaAs	80 nm, p, $4\cdot10^{19}$	
Collector	GaAs	700 nm, n, $1\cdot10^{16}$	EXTRINSIC COLLECTOR REMOVED
Etch-stop	$In_{0.48}Ga_{0.52}P$	50 nm, n, $5\cdot10^{18}$	
Sub-collector	GaAs	700 nm, n, $1\cdot10^{16}$	
COLLECTOR CONTACT			

Fig. 3. Layer structure of the simulated HBT.

The above equation shows that the first-order NQS correction can be added to a charge-conserving QS expression without destroying charge conservation. In case charge conservation is not needed, (26) can be implemented through nonlinear capacitance, as described in Section III-A. As shown in Fig. 2(b), three charge sources are used to represent the three derivatives in (26).

C. Transition to Voltage-Controlled Elements

The equivalent circuits in Fig. 2 include mainly current-controlled elements. Although current-controlled elements are available in modern circuit simulators (e.g., Advanced Design System (ADS),[1] APLAC[2]), they are not suitable for typical nodal analysis because branch currents are not readily available. Node voltages, on the other hand, are readily available, making voltage-controlled elements preferable for nodal analysis. Voltage control can be introduced to a current-controlled circuit by inserting a small current-sensing resistor in the controlling branch. For example, current-controlled $\tilde{I}_S$ in Fig. 2(a) can be brought under voltage control by introducing two resistors in series with Q_1 and Q_2 for sensing $\tilde{I}_1$ and $\tilde{I}_2$, respectively. The circuit in Fig. 2(b) can be similarly modified.

IV. Results and Discussion

Given difficulties in measuring high-speed transient waveforms with acceptable accuracy, we decided to verify the present modeling approach against physical device simulation (ATLAS).[3] Fig. 3 illustrates the generic design of the HBT used in the physical simulation. The emitter area of the simulated transistor is $1.4 \times 30\ \mu\mathrm{m}^2$. To simplify compact model extraction, only the intrinsic collector under the emitter is included in the simulation. The HBT has a relatively low Kirk threshold $(J_K \sim 15\ \mathrm{kA/cm^2})$ so that the high-current performance of the model can be readily tested. The simulated trends in *I–V* characteristics and S-parameters were consistent with that observed on typical InGaP HBTs. Fig. 4 shows bias dependence of the cutoff frequency f_T of the transistor. Special care was taken in order to capture all relevant physical mechanisms pertaining to

[1]Agilent Technol., Westlake Village, CA.

[2]APLAC Solutions Corporation, Atomitie 5 C, Helsinki, Finland.

[3]Silvaco International, Santa Clara, CA.

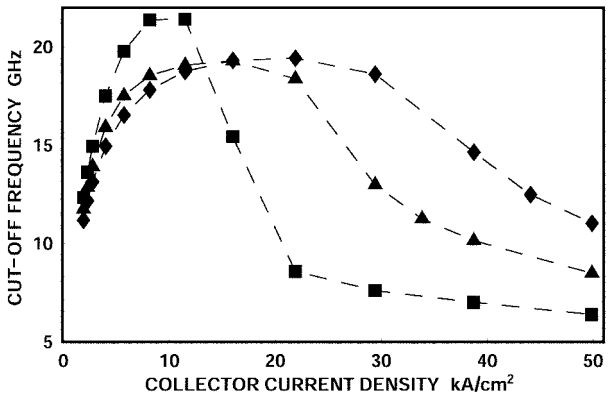

Fig. 4. Bias dependence of the cutoff frequency f_T of the simulated HBT, $V_{\rm CE}$ = (■)0.5V, (▲)1.5V, (♦)3V.

the HBT operation such as band alignment/grading, electron velocity overshoot, concentration-dependent mobility, bandgap narrowing, and surface/contact recombination.

The bias-dependent small-signal model of the HBT was extracted from the ATLAS-simulated S-parameters between 0.1–30 GHz under a bias of $V_{\rm CE} = 0$ to 5 V and $J_C = 0.1$ to $3J_K$. Details of the extraction procedure can be found elsewhere [20]. Fig. 5 illustrates the strong bias dependence of $\tau_C + \tau_D$ (effective collector transit time) and $C_{\rm BC}$ as simulated by using ATLAS.

Three different large-signal models were implemented in ADS and then used to simulate the HBT transient response. The models feature the same topology as in Fig. 1(b) and share definitions of I_F, $I_{\rm BE}$, and $Q_{\rm BE}$. The models differ only in implementation of dynamic currents $\tilde{I}_B$ and $\tilde{I}_C$. The first model, i.e., QSCC, is a regular QS model implemented by using the charge source Q according to (21). The model conserves charge and was extracted by fitting (22). The charge-conservation condition (23) was found to be valid below J_K, but was increasingly violated above J_K. The second model, i.e., NQSCC, introduces the first-order NQS correction to the QSCC model according to (29), while keeping the same function Q as in QSCC. Bias-dependent τ_1 in (29) was available as a result of small-signal model extraction. The third model, i.e., NQSNCC, also introduces the first-order NQS correction, but, unlike the first two models, it does not conserve charge and relies on nonlinear capacitors, as shown in Fig. 2.

The models were evaluated against ATLAS-simulated transient responses of a simple voltage-driven common-emitter amplifier with a resistive load R_L. Input excitation was a voltage step from $V_{\rm HI}$ down to 1.2 V with falling time $T_{\rm FALL}$. This produced a collector current transient from $I_{\rm HI}$ to 0, which is depicted in Figs. 6 and 7. The supply voltage was 2 V and the load resistor was chosen to produce a 0.5-V collector voltage swing, i.e., $R_L = 0.5/I_{\rm HI}$. Both $T_{\rm FALL}$ and $I_{\rm HI}$ were varied to evaluate the model's performance.

Fig. 6(a) shows collector current transients for $T_{\rm FALL} = 2$ ps and $I_{\rm HI} = 0.8J_K$. As expected, the NQS models predict similar roll off behaviors to that predicted by ATLAS, whereas the QS model predicts an abrupt shut off, which appears to be physically impossible. In addition, the QS model erroneously predicts a huge current spike at the beginning of the transient, which is

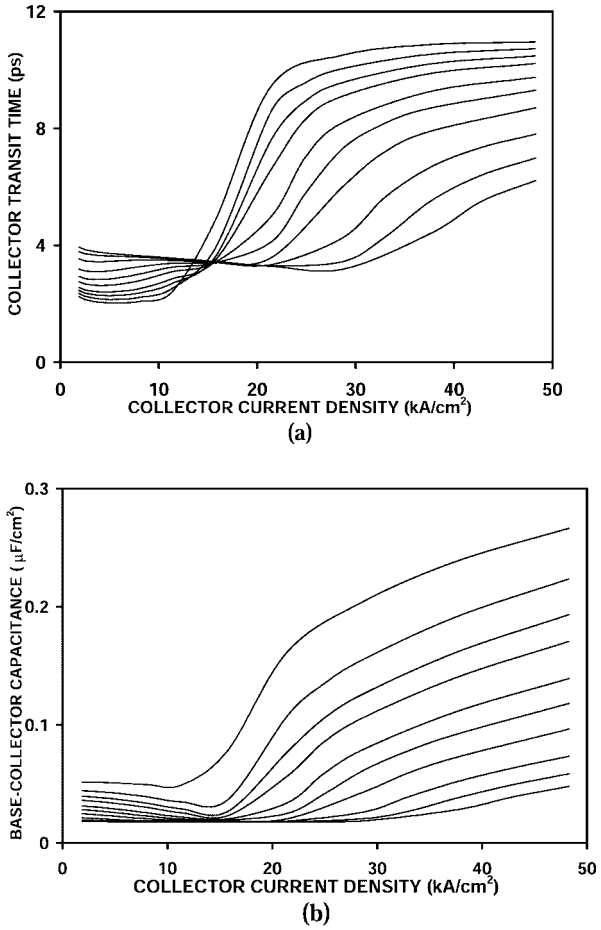

Fig. 5. Bias dependence of: (a) effective collector transit time $\tau_C + \tau_D$ and (b) base–collector capacitance $C_{\rm BC}$ as simulated by using ATLAS. $V_{\rm CE} = 0.5, 0.6, 0.7, 0.8, 1.0, 1.2, 1.5, 2.0, 2.5$, and 3.0 V top down.

largely corrected by the NQS models. Between the two NQS models, NQSCC is superior in predicting the rolloff behavior, while NQSNCC predicts a smaller spike. Similar observations were made in the case of $T_{\rm FALL} = 20$ ps, as shown in Fig. 6(b). Fig. 6(c) shows that, once $T_{\rm FALL}$ is increased to 200 ps, all models behave the same.

Fig. 7 shows collector current transients for $T_{\rm FALL} = 2$ ps with $I_{\rm HI}$ increased to 1.6 J_K or 2.4 J_K. With increasing $I_{\rm HI}$, the HBT's response slows, but the QS model predicts an opposite tendency. By contrast, the NQS models predict such a slowing tendency at least qualitatively. Between the two NQS models, the more complicated NQSNCC model does not demonstrate a clear advantage over the NQSCC model.

In general, charge-conserving versus noncharge-conserving modeling of semiconductor devices is a controversial topic beyond the scope of this paper. Noncharge-conserving models are commonly believed to be nonphysical, problematic in convergence, and, for these reasons, unsuitable for practical applications. Indeed, in many cases, charge conservation is dictated by physics so that development of a noncharge-conserving model cannot be justified. Examples include the gate terminal of a MOSFET (gate is isolated, therefore, the stored charge has no escape path) or the base terminal of an HBT (same reason, if recombination can be neglected). On the other hand, experi-

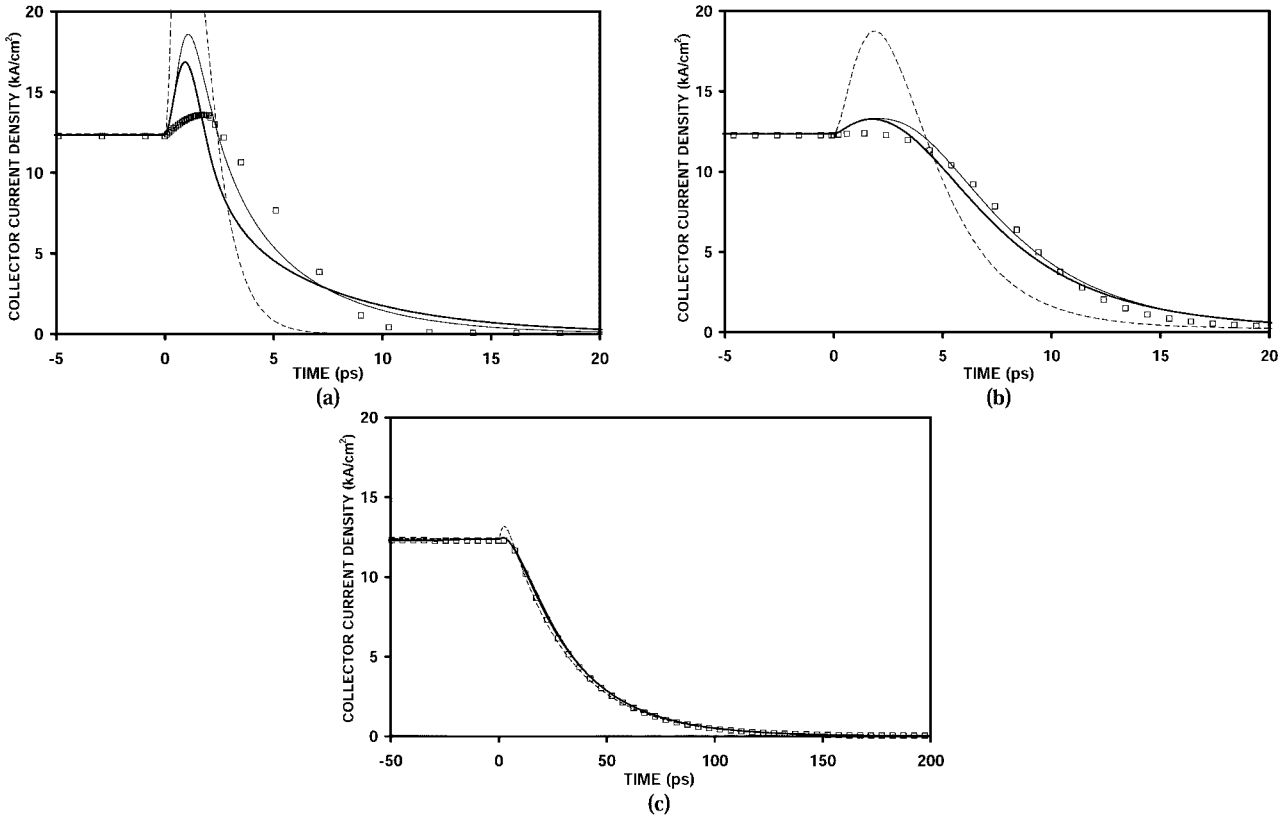

Fig. 6. Transient response of an HBT common-emitter amplifier simulated by using (- - -) QSCC, (—) NQSCC, (▬) NQSNCC, and (□) ATLAS models. $T_{\rm FALL}$ = (a) 2 ps, (b) 20 ps, and (c) 200 ps.

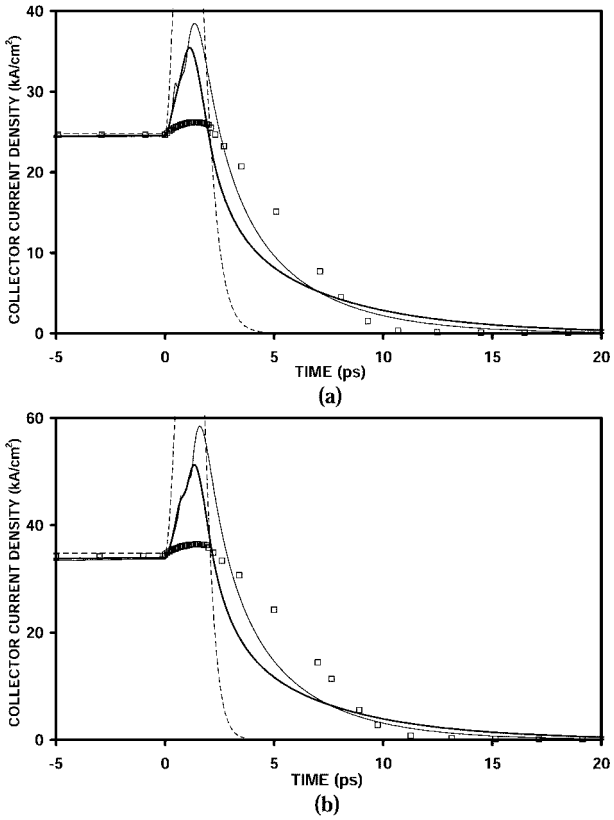

Fig. 7. Transient response of an HBT common-emitter amplifier simulated by using (- - -) QSCC, (—) NQSCC, (▬) NQSNCC, and (□) ATLAS models. $T_{\rm FALL} = 2$ps. $I_{\rm HI}$ = (a) $1.6\,J_K$ and (b) 2.4 J_K.

mental evidence of charge nonconservation has also been published. For example, [17] concluded that the drain terminal of a MESFET may not conserve charge. We are not currently aware of any theoretical proof of charge conservation for a device terminal that carries substantial conductive current, such as the drain of a MESFET or the collector of a BJT. In fact, the incremental charge approach used to derive the charge–source formalism can only be justified when the conductive current is negligible. We, therefore, believe that, troublesome as they are, noncharge-conserving models should not be categorically dismissed and should be constructively compared and evaluated against charge-conserving ones.

V. Conclusion

In summary, two possible approaches of large-signal implementation of NQS effects in bipolar transistors have been demonstrated. First-order NQS correction has been made to a QS model with and without charge conservation. The two resulted large-signal models have been evaluated against transient response predicted by using a physical device simulator. The results indicate significant improvement of the NQS models over the QS model, especially under rapid transients or high currents. The simpler charge-conserving NQS model has been found to be as accurate as the more complicated noncharge-conserving NQS model. Giving the charge-conserving model's smaller implementation effort and greater tendency to converge during circuit simulation, it is

the preferred approach for extending traditional compact QS models to higher frequencies.

ACKNOWLEDGMENT

The authors are grateful to the helpful comments of W. Curtice, W. R. Curtice Consulting, Washington Crossing, PA, D. Root, Agilent Technologies Inc., Santa Rosa, CA, and M. Shirokov, Ratheon RF Components, Andover, MA.

REFERENCES

[1] C. T. Sah, "The equivalent circuit model in solid-state electronics—III," *Solid State Electron.*, vol. 13, pp. 1547–1575, 1970.

[2] A. Pacelli, M. Mastrapasqua, and S. Luryi, "Generation of equivalent circuits from physics-based device simulation," *IEEE Trans. Computer-Aided Design*, vol. 19, pp. 1241–1250, Nov. 2000.

[3] J. A. Seitchik, A. Chatterjee, and P. Yang, "An accurate bipolar model for large signal transient and DC applications," in *Int. Electron Device Meeting Tech. Dig.*, 1987, pp. 244–247.

[4] J. A. Seitchik, "Comments on 'one-dimensional non-quasi-static models for arbitrary and heavily doped quasineutral layers in bipolar transistors'," *IEEE Trans. Electron Devices*, vol. 37, pp. 2108–2112, Sept. 1990.

[5] J. S. Hamel, "An accurate charge control approach for modeling excess phase shift in the base region of bipolar transistors," *IEEE Trans. Electron Devices*, vol. 43, pp. 1092–1098, July 1996.

[6] B. S. Wu and F. A. Lindholm, "One-dimensional all injection nonquasi-static models for arbitrary doped quasi-neutral layers in bipolar junction transistors including plasma-induced energy-gap narrowing," *IEEE Trans. Electron Devices*, vol. 37, pp. 250–261, Jan. 1990.

[7] N. F. Rinaldi, "Modeling of small-signal minority-carrier transport in bipolar devices at arbitrary injection levels," *IEEE Trans. Electron Devices*, vol. 45, pp. 1501–1510, July 1998.

[8] W. Liu, *Handbook of III–V Heterojunction Bipolar Transistors*. New York: Wiley, 1998, pp. 650–654.

[9] M. Sipilä, V. Porra, and M. Valtonen, "Improved description of base dynamics in the modeling of bipolar transistors," *Int. J. Circuit Theory Applicat.*, vol. 17, pp. 465–482, 1989.

[10] H. M. Rein and M. Schröter, "A compact physical large-signal model for high-speed bipolar transistors at high current densities," *IEEE Trans. Electron Devices*, vol. ED-34, pp. 1752–1761, Aug. 1987.

[11] P. Roblin, S. C. Kung, and W.-R. Liou, "Improved small-signal equivalent circuit model and large-signal state equations for the MOSFET/MODFET wave equation," *IEEE Trans. Electron Devices*, vol. 38, pp. 1706–1718, Aug. 1991.

[12] P. Antognetti and G. Massobrio, *Semiconductor Device Modeling With SPICE*. New York: McGraw-Hill, 1987, ch. 2.

[13] J. G. Fossum and S. Veeraraghavan, "Partitioned-charge-based modeling of bipolar transistors for nonquasi-static circuit simulation," *IEEE Electron. Device. Lett.*, vol. EDL-7, pp. 652–654, Dec. 1986.

[14] J. S. Hamel, "Comment on 'modeling of small-signal minority carrier transport in bipolar devices at arbitrary injection levels'," *IEEE Trans. Electron Devices*, vol. 49, pp. 1839–1841, Oct. 2002.

[15] N. Rinaldy, "Reply to comments on 'modeling of small-signal minority carrier transport in bipolar devices at arbitrary injection levels'," *IEEE Trans. Electron Devices*, vol. 49, pp. 2371–2373, Dec. 2002.

[16] Y. Betser and D. Ritter, "Reduction of the base–collector capacitance in InP/GaInAs heterojunction bipolar transistors due to electron velocity modulation," *IEEE Trans. Electron Devices*, vol. 46, pp. 628–633, Apr. 1999.

[17] D. E. Root and S. Fan, "Experimental evaluation of large-signal modeling assumptions based on vector analysis of bias-dependent S-parameter data from MESFET's and HEMTs," in *IEEE MTT-S Int. Microwave Symp. Dig.*, 1992, pp. 255–259.

[18] Y. P. Tsividis, *Operation and Modeling of the MOS Transistor*, 2nd ed. New York: McGraw-Hill, 1999.

[19] D. E. Root, "Nonlinear charge modeling for FET large-signal simulation and its importance for IP3 and ACPR in communication circuits," in *Proc. 44th IEEE Midwest Circuits Systems Symp.*, vol. 2, 2001, pp. 768–772.

[20] S. V. Cherepko, M. S. Shirokov, J. C. M. Hwang, and A. Brandstaedter, "Improved large-signal model and model extraction procedure for InGaP/GaAs HBT's under high-current operations," in *IEEE MTT-S Int. Microwave Symp. Dig.*, 2001, pp. 671–674.

Sergey V. Cherepko (S'99) received the B.S. and M.S. degrees in electrical engineering from the Moscow Engineering Physics Institute, Moscow, Russia, in 1992 and 1995, respectively, and the Ph.D. degree in electrical engineering from Lehigh University, Bethlehem PA, in 2003.

He is currently a Visiting Research Scientist with the Center for Optical Technologies, Lehigh University. His research interests include advanced compact modeling of semiconductor devices at RF frequencies.

James C. M. Hwang (M'81–SM'82–F'94) received the B.S. degree in Physics from the National Taiwan University, Taipei, Taiwan, R.O.C., in 1970, and the M.S. and Ph.D. degrees in materials science and engineering from Cornell University, Ithaca, NY, in 1973 and 1976, respectively.

He possesses 12 years of industrial experience with IBM, AT&T, GE, and GAIN. In 1988, he joined Lehigh University, Bethlehem, PA, as Professor of electrical engineering and Director of the Compound Semiconductor Technology Laboratory. In 2002, he helped establish the $40 million Center for Optical Technologies at Lehigh University and Pennsylvania State University, and served as the interim Director for six months. He has been a Visiting Professor with the Nanyang Technological University, Nanyang, Singapore, and Shanghai Jiaotong University, Shanghai, China. He has been a consultant for the U.S. Government and many electronic companies in the area of RF/microwave devices and integrated circuits. He co-founded GAIN and QED and saw the former go bankrupt, while the latter become a public company (IQE). He has authored or coauthored over 150 technical papers. He holds four U.S. patents.